PRAMANA — journal of physics

© Indian Academy of Sciences

Vol. 82, No. 6
June 2014
pp. 1061–1074

Switching behaviour of nonlinear Mach–Zehnder interferometer based on photonic crystal geometry

MAN MOHAN GUPTA and S MEDHEKAR*

Centre for Applied Physics, Central University of Jharkhand, Ranchi 835 205, India
*Corresponding author. E-mail: smedhekarbit@gmail.com

MS received 23 April 2013; revised 20 October 2013; accepted 25 November 2013
DOI: 10.1007/s12043-014-0705-x; ***e*Publication:** 15 May 2014

Abstract. Nonlinear Mach–Zehnder interferometer (NMZI) created with photonic crystal waveguides (PCW) and with Kerr-type nonlinearity has been investigated in this paper. The NMZI has been simulated using two-dimensional finite difference time domain (2D-FDTD) method. Input verses output (I/O) characteristics have been obtained for different lengths of the nonlinear arm, nonlinear coefficients of the nonlinear arm, wavelengths of the input beam, sizes of defect rods and NMZI offset. The results obtained are compared with earlier published results of NMZI created with conventional step index waveguides (SIW). It is shown that all useful features of light switching offered by SIW-based NMZIs are also possible with PCW-based NMZIs of extremely small dimensions. Moreover, PCW-based NMZIs offer additional useful feature not available with SIW-based NMZIs.

Keywords. Mach–Zehnder interferometer; photonic crystal; Kerr effect; nonlinear optical devices; all-optical switching; self-phase modulation.

PACS Nos 42.65.Pc; 42.65.Wi; 42.82.–m

1. Introduction

One of the top-listed and extensively investigated components for optical devices is Mach–Zehnder interferometer (MZI) [1,2]. When MZI is fabricated with one of its arm made of a nonlinear material, it becomes an all-optical switching device and is called as nonlinear Mach–Zehnder interferometer (NMZI). NMZI using the optical Kerr effect is more suitable for faster transmission systems due to its ultrafast response. Multiplexing and modulation [3], WDM applications [4], optical power limiter [5], signal amplifier [6] are some of the examples of applications of MZI structure.

NMZI structure has also been investigated for all-optical logic [7–10] due to its application in telecommunication systems. All-optical AND gate can perform the bit-level functions like packet-header modification, data-integrity verification and address

recognition. The all-optical XOR gate is a key technology to implement primary systems for binary address and header recognition, binary addition and counting, decision and comparison, encoding and encryption, and pattern matching.

Photonic crystal (periodic structures of dielectric) is a subject of recent interest in optical communication and computing. Photonic crystals, in which propagation of light for frequencies within a photonic band gap is prohibited, allow for entirely new ways to control and manipulate light [11,12]. Further miniaturization and lowering of operating powers of ultrahigh speed all-optical devices is possible using photonic crystals to make them truly practicable. Various schemes have been proposed to realize all optical components using photonic crystal geometries [13–18].

It would, therefore be a wise idea to explore switching of light in a NMZI created with PCWs in detail. In view of this, the present paper investigates a Kerr-type NMZI created with PCWs. Using 2D-FDTD, a thorough investigation has been carried out on the I/O characteristics by varying different parameters like length of the arms, nonlinear coefficient of the nonlinear arm, wavelength of the input beam, size of the defect rods and NMZI offset.

Similar investigations have been carried out earlier [19] on a NMZI created with step index waveguides (SIW). However, the investigation in the present paper is motivated by the hope that the use of PCWs to create a NMZI would allow exploiting the advantages of both photonic crystal and Mach–Zehnder interferometer.

The results obtained in the present paper for PCW-based NMZI are compared with the results of SIW-based NMZI [19]. This paper is intended to develop a physical understanding of the switching behaviour of the PCWs-based NMZIs that would be helpful to the scientists/theoreticians as well as engineers and fabricators.

2. Device

For carrying out a thorough investigation on the switching behaviour of PCW-based NMZI, we consider the novel structure of ref. [20]. Figure 1 shows its schematic. There are two 3 dB directional couplers DC1 and DC2 as shown. It has two input ports P1 and P2 and two output ports P3 and P4. When light is injected at P1 or P2, the output can be obtained at P3 and P4.

A 2D square lattice version of figure 1 that consists of infinitely long circular rods of refractive index ($n_H = 3.5$), embedded in a background of refractive index ($n_L = 1.5$) is shown in figure 2a. Radius (R) of the rods is $0.25a$. Defect rods are having radius (r) equal to $0.15a$, where a is the lattice constant. This geometry supports the bandgap for transverse electric (TE) mode, which extends from $a/\lambda = 0.24$ to 0.29, where λ is the free-space wavelength. Continuous wave (CW) Gaussian beams of normalized frequency $a/\lambda = 0.263$, is chosen to be launched at input port. Nonlinear defect rods are marked as light gray circles. The lengths of directional couplers (L_{DC}) and nonlinear arm (L_{NLA}) are $15a$ and $131a$, respectively. Lattice constant (a) is 0.4 μm.

When an input beam is launched at port P1, it splits into two equal parts after passing through the first directional coupler. One part propagates through the nonlinear arm (NLA) and its counterpart propagates through linear arm (LA). The part propagating

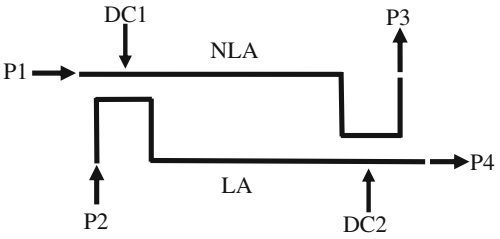

Figure 1. The schematic of the NMZI structure/device. There are two 3 dB directional couplers DC1 and DC2.

through the NLA experiences self-phase modulation (SPM). If the optical path difference of the split parts is equal to zero or integral multiple of the wavelength, they recombine constructively at P4 as shown by the steady-state field in figure 2b which has been obtained using FDTD as mentioned below. If their optical paths differ by half integer of the wavelength, they recombine constructively at P3 (figure 2c). It happens the same way if the input is launched at P2 except that the output ports are reversed.

3. Numerical method and analysis

In order to investigate switching behaviour of the above-mentioned device, we use finite difference time domain (FDTD) method which is the most popular and well-known technique to solve a variety of electromagnetic problems. Maxwell's curl equations in source-free region can be arranged in the following form [21]:

$$\frac{\partial H}{\partial t} = -\frac{1}{\mu}\nabla \times E - \frac{\rho}{\mu}H, \tag{1}$$

$$\frac{\partial E}{\partial t} = \frac{1}{\varepsilon}\nabla \times H - \frac{\sigma}{\varepsilon}E, \tag{2}$$

where ε, μ, σ and ρ are the permittivity, permeability, electric conductivity and equivalent magnetic conductivity of the material, respectively.

For 2D-FDTD calculations, fields can be classified into two modes, transverse electric (TE) mode and transverse magnetic (TM) mode, depending on the direction of electric field. We have considered incident electric field parallel to y-axis (TE mode) and the plane of propagation is the x-z plane. As considered, the structure extends to infinity in y direction, $(\partial/\partial y) = 0$ and only three components E_y, H_x and H_z exist for 2D-TE mode in wave propagation [22]. Equations (1) and (2) can be descretized in position and time using Yee's Algorithm [23]. Hence, 2D-FDTD stepping formulae for TE mode can be written as follows [24]:

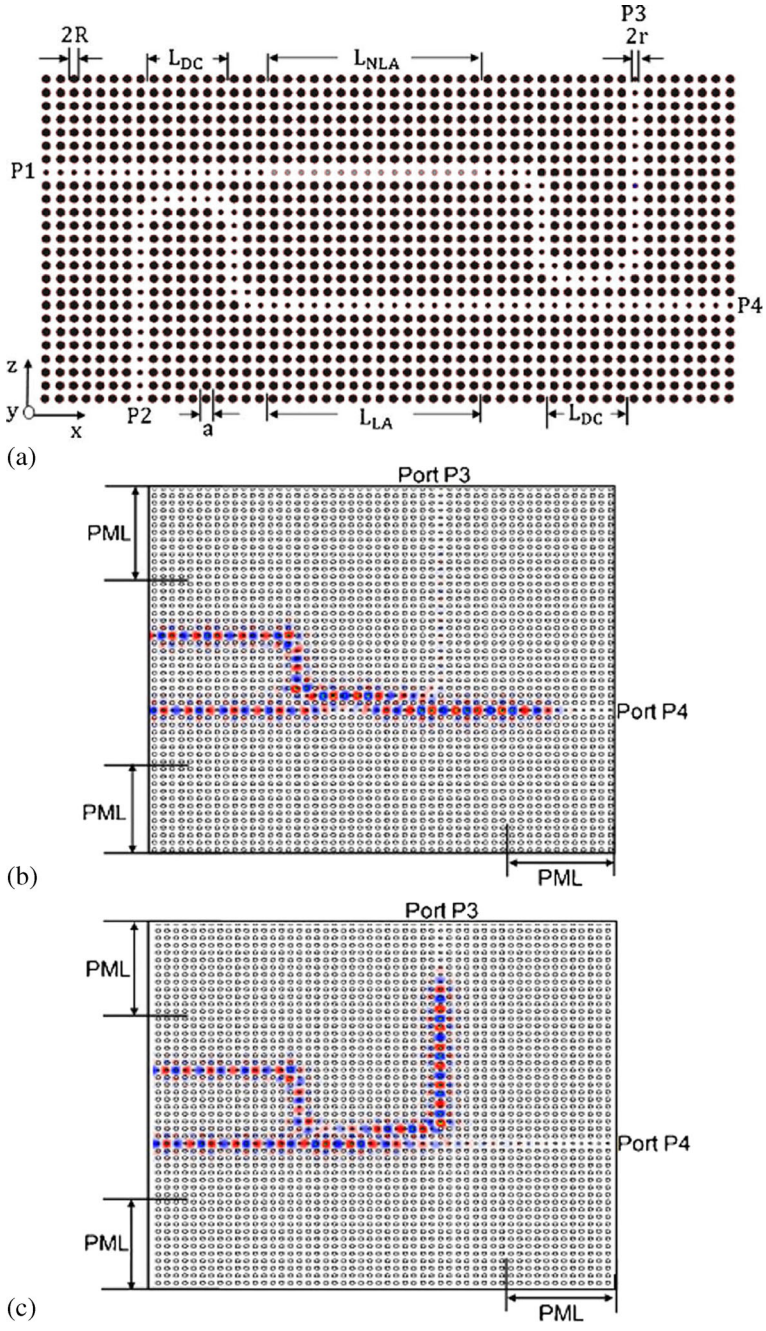

Figure 2. (**a**) Nonlinear Mach–Zehnder interferometer based on 2D square lattice photonic crystal geometry of infinitely long dielectric rods. (**b**) Steady-state field pattern at output ports when optical path difference of the split parts is equal to zero or integral multiple of the wavelength. (**c**) Steady-state field pattern at output ports when optical path difference of the split parts is equal to half integer of the wavelength.

$$E_y\left|{}^{n+\frac{1}{2}}_{i-\frac{1}{2},k+\frac{1}{2}}\right. = \left(\frac{2\Delta t}{2\varepsilon+\sigma\Delta t}\right) \times \left(\frac{H_x\left|{}^{n}_{i-\frac{1}{2},k+1}\right. - H_x\left|{}^{n}_{i-\frac{1}{2},k}\right.}{\Delta z} - \frac{H_z\left|{}^{n}_{i,k+\frac{1}{2}}\right. - H_z\left|{}^{n}_{i-1,k+\frac{1}{2}}\right.}{\Delta x}\right) + \left(\frac{2\varepsilon-\sigma\Delta t}{2\varepsilon+\sigma\Delta t}\right) E_y\left|{}^{n-\frac{1}{2}}_{i-\frac{1}{2},k+\frac{1}{2}}\right. \tag{3}$$

$$H_x\left|{}^{n+1}_{i-\frac{1}{2},k+1}\right. = \left(\frac{2\Delta t}{2\mu+\rho\Delta t}\right)\left(\frac{E_y\left|{}^{n+\frac{1}{2}}_{i-\frac{1}{2},k+\frac{3}{2}}\right. - E_y\left|{}^{n+\frac{1}{2}}_{i-\frac{1}{2},k+\frac{1}{2}}\right.}{\Delta z}\right) + \left(\frac{2\mu-\rho\Delta t}{2\mu+\rho\Delta t}\right) H_x\left|{}^{n}_{i-\frac{1}{2},k+1}\right. \tag{4}$$

$$H_z\left|{}^{n+1}_{i,k+\frac{1}{2}}\right. = -\left(\frac{2\Delta t}{2\mu+\rho\Delta t}\right)\left(\frac{E_y\left|{}^{n+\frac{1}{2}}_{i+\frac{1}{2},k+\frac{1}{2}}\right. - E_y\left|{}^{n+\frac{1}{2}}_{i-\frac{1}{2},k+\frac{1}{2}}\right.}{\Delta x}\right) + \left(\frac{2\mu-\rho\Delta t}{2\mu+\rho\Delta t}\right) H_z\left|{}^{n}_{i,k+\frac{1}{2}},\right. \tag{5}$$

where i and k denote the discretized grid point in x–z planes respectively, index n denotes the discrete time step. Δx and Δz are the intervals between two neighbouring grid points along the x and z directions respectively and Δt is the time interval. PML absorbing boundary conditions are used [25,26] in order to remove unwanted reflection from the boundaries.

As one of the arms of the considered NMZI is with Kerr-type nonlinearity, we incorporate nonlinearity in the nonlinear arm as below.

$$n = n_H + \Delta n. \tag{6}$$

Here n_H is the linear refractive index and Δn is the change in the refractive index of the nonlinear material induced by electric field of the input beam and can be written as [27]

$$\Delta n = n_2 I, \tag{7}$$

where n_2 is the Kerr coefficient of the nonlinear material, I is the intensity of the launch beam. Intensity of launch beam is proportional to $|E|^2$, where E is the electric field distribution of the launch beam. Third-order nonlinear susceptibility (χ^3) is related to the Kerr coefficient n_2 as [28]

$$\chi^3 = \frac{4n_2 n_{H^2}}{3Z_0}, \tag{8}$$

where Z_0 is the impedance of free space.

Parameters of AlGaAs have been considered for the present investigations which has nearly instantaneous nonlinearity with Kerr coefficient $n_2 = 1.5 \times 10^{-17}$ m^2/W below the electronic bandgap at 1.55 μm [13,29].

Numerical investigations have been carried out with help of FullWAVE module (based on FDTD technique) of RSOFT Design Group, NY-USA. The grid size in x and z directions is taken as $a/20$, i.e. 20 lattice points per unit cell in the present investigation. Simulation domain is surrounded by the PML layers and the width of the PML region is chosen as 5 μm.

3.1 *Switching behaviour by varying the length of the nonlinear arm*

To investigate the switching behaviour, we launch CW Gaussian input at P1. We gradually increase the input intensity at P1 and examine the output at P3 and P4. Figure 3a shows variation of output at P3 and P4 with input at P1. When input intensity is vanishingly small, zero path difference in the split parts of the input beam makes the whole input appearing at port P4 leaving no light at port P3. When the input intensity is gradually increased, the magnitude of self-phase modulation (SPM) of the part propagating through NLA increases and the input gradually switches to port P3. At a particular input intensity the magnitude of the self-phase modulation is such that optical path difference of the split parts differ by half of the wavelength and the whole of the input beam appears at P3 leaving no light at P4. If the input intensity at P1is further increased, field at port P3 decreases, while, it increases at P4.

To understand the effect of nonlinear arm length (NLA) on the switching of the NMZI, transmission coefficient (at P4) with input intensity (at P1) is plotted in figure 3a as shown by dashed, solid and dotted curves for the length of nonlinear arm L_{NLA} equal to $109a$, $120a$ and $131a$, respectively. Dashed, solid and dotted curves with dark circles show the same at P3. Figure 3b shows I/O characteristics corresponding to figure 3a.

It is obvious from the figure that transmission coefficient oscillates between maxima and minima with the increase in input intensity at port P1. It is also clear from the figure that higher input intensity is required for the shorter nonlinear arm length to obtain the complete switching. The reason for what is mentioned above is easily understandable. As the length of the NLA increases, the accumulated phase change at the output directional coupler of the NMZI also increases, and hence, switching occurs at lower input intensity.

The above behaviour of the PCW-based NMZI is similar to that of a SIW-based NMZI [19]. However, a quick estimate suggests that for the same magnitude of nonlinear coefficients, the ratio of the required input intensities in SIW-based NMZI and PCW-based NMZI would be $\sim$0.1. Hence, the ratio of powers would be $\sim$1 as the ratio of the waveguide widths is $\sim$10. It is worth emphasizing that the NMZI length in SIW-based NMZI is of the order of 5000 μm, while in PCW-based NMZI it is merely 75 μm. It is also worth mentioning that the length of a SIW-based NMZI can be increased or decreased arbitrarily, whereas the length of a PCW-based NMZI can be increased or decreased in steps of the unit cell.

3.2 *Switching behaviour with different nonlinearity coefficients*

To examine the effect of nonlinearity coefficient on the switching behaviour of NMZI, different nonlinearity coefficients have been considered with other parameters of figure 2a.

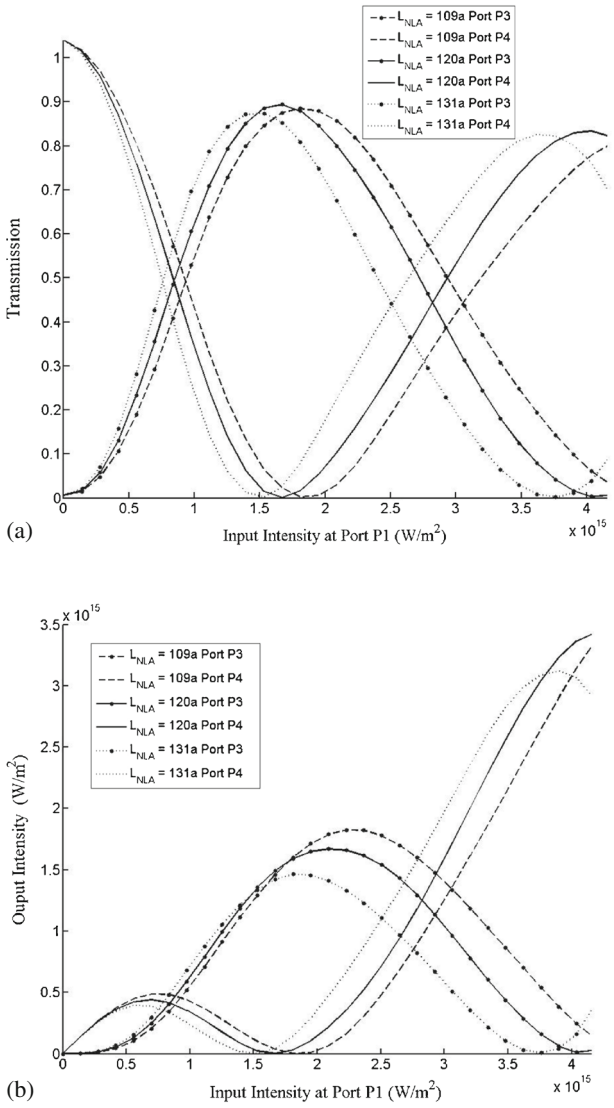

Figure 3. (**a**) Variation of transmission at P3 and P4 with input intensity at P1 for the length of NLA (L_{NLA}) =109*a*, 120*a* and 131*a*. (**b**) Variation of output intensity at P3 and P4 with input intensity at P1 for the length of NLA (L_{NLA}) = 109*a*, 120*a* and 131*a*.

Transmission vs. input and I/O characteristics obtained at port P4 are shown in figures 4a and 4b respectively. Dashed, solid and dotted curves are obtained for nonlinearity coefficients equal to 1.2×10^{-17}, 1.5×10^{-17} and 1.8×10^{-17} m^2/W respectively. The same at port P3 is shown by dashed, solid and dotted curves with dark circles. It is evident from figures 4a and 4b that output switching power decreases with increase in nonlinearity

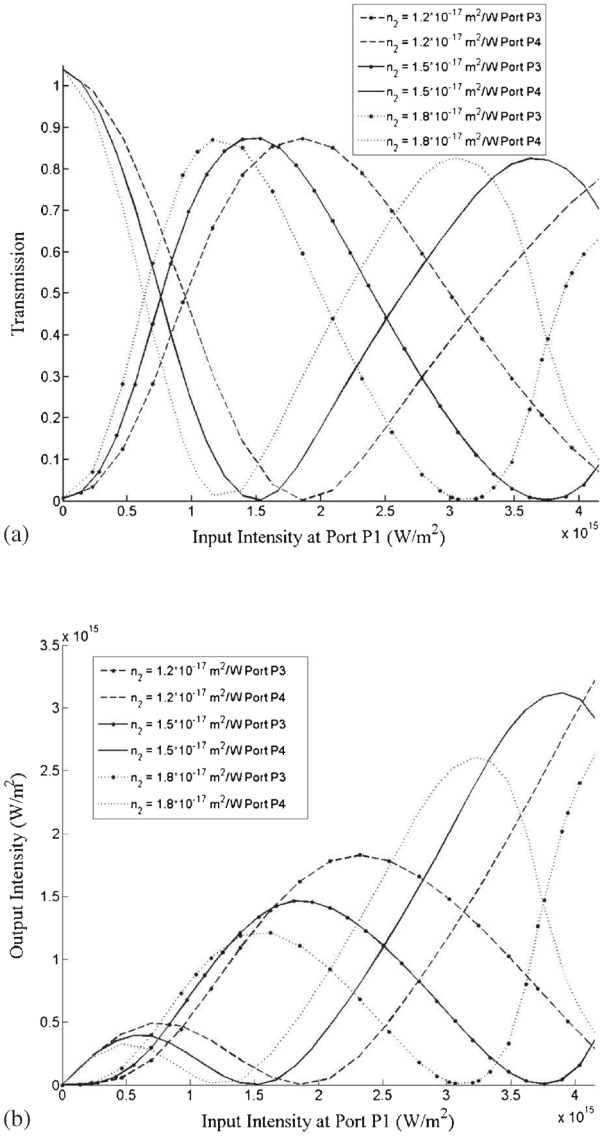

Figure 4. (**a**) Variation of transmission at P3 and P4 with input intensity at P1 for nonlinearity coefficients equal to 1.2×10^{-17}, 1.5×10^{-17} and 1.8×10^{-17} m^2/W. (**b**) Variation of output intensity at P3 and P4 with input intensity at P1 for nonlinearity coefficients $= 1.2 \times 10^{-17}$, 1.5×10^{-17} and 1.8×10^{-17} m^2/W.

coefficient. This is due to the fact that effect of nonlinearity increases with the nonlinear coefficient.

The switching behaviour of the PCW-based NMZI matches with the SIW-based NMZI here as well [19].

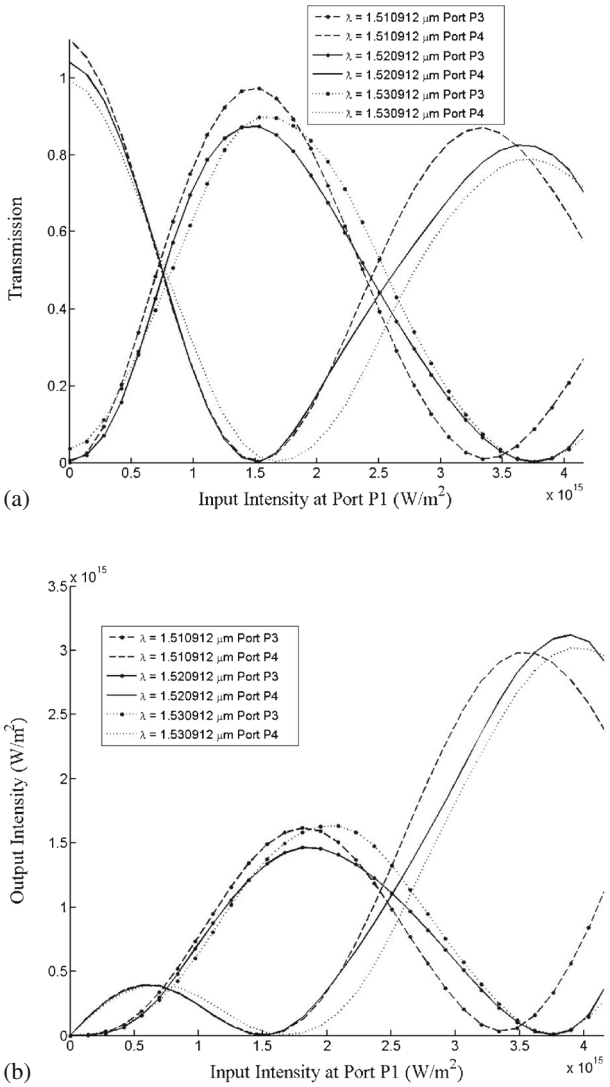

Figure 5. (**a**) Variation of transmission at P3 and P4 with input intensity at P1 for input wavelengths (λ) = 1.510912, 1.520912 and 1.530912 μm. (**b**) Variation of output intensity at P3 and P4 with input intensity at P1 for input wavelengths (λ) = 1.510912, 1.520912 and 1.530912 μm.

3.3 *Switching behaviour with varying wavelength*

Wavelength of the input beam plays an important role in the photonic crystal structures. Normalized wavelengths ranging from 0.24 to 0.29 are forbidden in the considered structure in case of TE polarization. Therefore, those could be guided in the line defect (waveguide) of the structure. The guidance would be weaker or even vanish for the wavelengths other than the mentioned range.

Keeping all other parameters same as in figure 2a, transmission coefficients and output intensities at ports P3 and P4 with varying input intensities $\left(0\text{–}4.15 \times 10^{15}\ \mathrm{W/m^2}\right)$ at P1 are plotted in figures 5a and 5b, respectively. Dashed, solid and dotted curves show device characteristics for input wavelength (λ) 1.510912, 1.520912 and 1.530912 μm respectively obtained at port P4. Dashed, solid and dotted curves with dark circles show the same at P3. It is seen that the switching occurs at lower intensity if the wavelength of the input is decreased.

The behaviour of PCW-based NMZI matches yet again with that of a SIW-based NMZI [19]. However, possible variation in the wavelength in both cases is limited by the fact that injected wavelength should propagate as the fundamental mode in the NMZI. As the light guidance mechanism in a PCW is different from SIW, the PCW offers narrower range of wavelength for the fundamental mode propagation.

3.4 *Effect of change of offset on switching behaviour*

For a low intensity input, whole input launched at port P1, appears at port P4 leaving zero output at port P3. It is called as zero offset condition [19]. In the considered structure, zero offset condition may be obtained by keeping the same value of linear refractive index of the rods of linear and nonlinear arms ($n_H = 3.5$). The offset of a NMZI can be changed by slightly changing the linear refractive index of one of the two arms. Change of offset is an attractive feature as it offers adjustment of operating powers of a NMZI device [19].

In this section, we have investigated the effect of change of offset on the switching behaviour of the NMZI. For this purpose, we consider n_H of the rods of the linear arm equal to 3.495, 3.5 and 3.505 and obtain I/O characteristics at P3 and P4 by varying the input at port P1 as shown in figures 6a and 6b. Dashed, solid and dotted curves in these figures show output at P4 for $n_H = 3.495$, 3.5 and 3.505 respectively, while, the same with dark circles show output at P3.

It is clear from figures 6a and 6b that the switching power of the NMZI can be increased by increasing the value of n_H of the linear arm. This is similar to the switching behaviour of SIW-based NMZI.

In the above sections, all the changes considered in the PCW-based NMZI for the investigation of its switching behaviour were also possible in a SIW-based NMZI. However, the change considered in the following section is only possible with a PCW-based NMZIs.

3.5 *Effect of defect rod size on switching behaviour*

In order to create a waveguide in PCs, a series of defects is used. In rod-type PCs, these defects can be introduced either by removing a rod, or increasing/reducing the size of the rod. In the NMZI considered, the waveguide has been created by using defect rods. It is therefore worth investigating the effect of the size of the defect rods on switching behaviour of the NMZI.

We choose different radii (r) of the defect rods. Figure 7a shows variation of transmission at ports P3 and P4 with varying input intensity given at port P1. Dashed, solid and dotted curves show the variation of output at port P4 for the defect rods of size $r =$

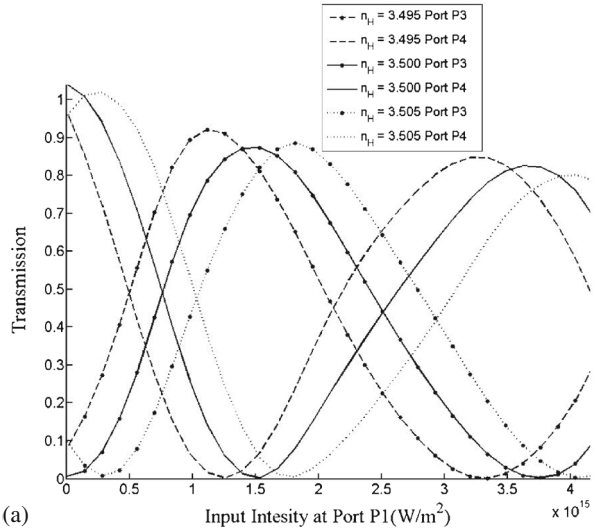

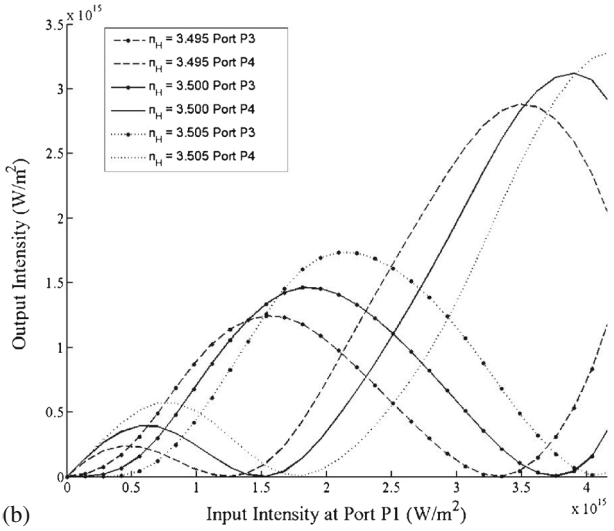

Figure 6. (**a**) Variation of transmission at P3 and P4 with input intensity at P1 for $n_H = 3.495$, 3.5 and 3.505 of linear arm rods. (**b**) Variation of output intensity intensity at P3 and P4 with input intensity at P1 for $n_H = 3.495$, 3.5 and 3.505 of linear arm rods.

0.145a, 0.150a and 0.155a respectively. Dashed, solid and dotted curves with dark circles show the same at port P3. Figure 7b shows the variation of output intensities at ports P3 and P4 corresponding to figure 7a.

One can note that by changing the dimension of the defect rod one can significantly change the switching power of a NMZI. Therefore, PCW-based NMZI offers extra liberty

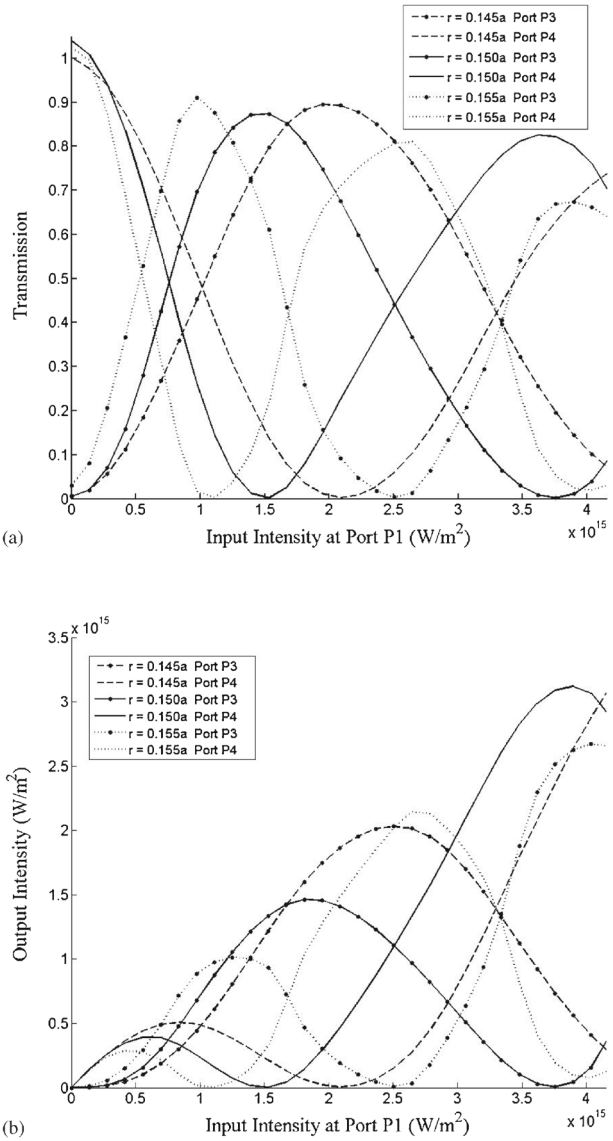

Figure 7. (**a**) Variation of transmission at P3 and P4 with input intensity at P1 for the defect rod size $r = 0.145a$, $0.150a$ and $0.155a$. (**b**) Variation of output intensity at P3 and P4 with input intensity at P1 for the defect rod size $r = 0.145a$, $0.150a$ and $0.155a$.

for manipulation in the operating powers of the device which is not possible in a SIW-based NMZI.

We must add here that while the above-mentioned feature is advantageous in terms of manipulating device operating power, it would require precise fabrication of the crystal with proper dimensions/parameters. In general, fabrication of PCW-based devices

requires better control on dimensions/parameters as compared to SIW-based devices to obtain the desired performance.

4. Conclusion

Nonlinear Mach–Zehnder interferometer with Kerr-type nonlinearity and which is based on photonic crystal geometry has been investigated using two-dimensional finite difference time domain method (2D-FDTD). A thorough investigation on input vs. output characteristics was carried out by varying different parameters like length of nonlinear arm, refractive index of the linear arm, wavelength of the input beam, nonlinear coefficient of the material of the nonlinear arm and size of the PC defect rods. The obtained results were compared with the earlier published results obtained with SIW-based NMZI. It is found that all useful features of light switching available with SIW-based NMZIs are also available with PCW-based NMZIs. In addition, the following conclusions can be drawn from the present investigation:

(i) For the same magnitude of nonlinear coefficients, switching of light could be obtained at the same operating power in a PCW-based NMZI which is ten times smaller in size as compared to a SIW-based NMZI.
(ii) Qualitative change in the switching behaviour in a PCW-based NMZI is similar to a SIW-based NMZI when parameters like length of nonlinear arm, refractive index of the linear arm, wavelength of the input beam and nonlinear coefficient are changed.
(iii) In PCW-based NMZI switching power could be changed significantly by merely changing the size of the defect rods which is a very attractive feature not available with SIW-based NMZIs. However, fabrication of such devices requires precise control on dimensions/parameters.

Acknowledgements

Authors acknowledge helpful discussions on photonic crystals with Dr Achanta Venugopal, Department of Condensed Matter Physics and Materials Science, Tata Institute of Fundamental Research, Mumbai. Authors also acknowledge the anonymous reviewer for invaluable comments to improve the presentation. MMG acknowledges Birla Institute of Technology, Mesra, Ranchi, India for Institute fellowship during Oct. 2012-Sept. 2013. SM acknowledges funding from Department of Science & Technology (DST), India (SR/S2/LOP-0025/2012).

References

[1] A Srivastava and S Medhekar, *Opt. Laser Technol.* **43**, 29 (2011)
[2] A Srivastava and S Medhekar, *Opt. Laser Technol.* **43**, 1208 (2011)
[3] P B Hansen and A H Gnauck, *IEEE Phot. Tech. Lett.* **4**, 592 (1992)
[4] N Yoshimoto, Y Shibata, S Oku, S Kondo and Y Noguchi, *IEEE Phot. Tech. Lett.* **10**, 531 (1998)

[5] N Pleros, G T Kanellos, C Bintjas, A Hatziefremidis and H Avramopoulos, *IEEE Phot. Tech. Lett.* **16**, 2350 (2004)
[6] A Srivastava, M M Gupta and S Medhekar, *Opt. Laser Technol.* **44**, 492 (2011)
[7] T Yabu, M Geshiro, T Kitamura, K Nishida and S Sawa, *IEEE J. Quant. Elec.* **38**, 37 (2002)
[8] S Medhekar and P P Paltani, *Fib. Inte. Opt.* **28**, 229 (2009)
[9] S Medhekar and P P Paltani, *Fib. Inte. Opt.* **28**, 268 (2009)
[10] S K Garai and S Mukhopadhyay, *Opt. Laser Technol.* **42**, 1122 (2010)
[11] S G Johnson, P R Villeneuve, S Fan and J D Joannopoulos, *Phys. Rev. B* **62**, 8212 (2000)
[12] J D Joannopoulos, P R Villeneuve and S Fan, *Nature* **386**, 143 (1997)
[13] M F Yanik, S Fan, M Soljacic and J D Joannopoulos, *Opt. Lett.* **28**, 2506 (2003)
[14] Z Wang and S Fan, *Opt. Lett.* **30**, 1989 (2005)
[15] Y Qu, H Ren and C Jiang, *IEEE Quant. Electron.* **43**, 974 (2007)
[16] Y Zhang, Y Zhang and B Li, *Opt. Exp.* **15**, 9287 (2007)
[17] Z H Zhu, W M Ye, J R Ji, X D Yuan and C Zen, *Opt. Exp.* **14**, 1783 (2006)
[18] H Zhou, K F Zhou, W Hu, Q Guo, S Lan, X S Lin and A V Gopal, *J. Appl. Phys.* **99**, 123111 (2006)
[19] A Srivastava, P P Paltani and S Medhekar, *Pramana – J. Phys.* **74**, 575 (2010)
[20] T Fujisawa and M Koshiba, *J. Light. Technol.* **24**, 617 (2006)
[21] A Taflove and S C Hagness, *Computational electrodynamics: The finite difference time-domain method*, 3rd edn (Artech House, Norwood, MA, 2005) p. 53
[22] S T Chu and S K Chaudhuri, *J. Lightwave Technol.* **7**, 2033 (1989)
[23] K S Yee, *IEEE Trans. Antennas Prop.* **14**, 302 (1966)
[24] M Benavides, M Alvarez, C Calderón, J Sosa, M Galaz, M Rodriguez, M Enciso and C Marquez, *Rev. Mex. Fis. E* **57**, 25 (2011)
[25] J P Berenger, *J. Comp. Phys.* **127**, 363 (1996)
[26] J P Berenger, *J. Comp. Phys.* **114**, 185 (1994)
[27] K Okamoto, *Fundamentals of optical waveguides* (Academic Press, USA, 2002) p. 274
[28] D C Hutchings, *IEEE J. Sele. Top. Quant. Elec.* **10**, 1124 (2004)
[29] M N Islam, C E Soccolich, R E Slusher, A F J Levi, W S Hobson and M G Young, *J. Appl. Phys.* **71**, 1927 (1992)